Comparing meshless methods with the finite element method for application of a bio-inspired remodelling algorithm intended to design bone scaffold

A.I.Pais [1], F.J.L.Alves [1], J. Belinha [2]

[1]INEGI Institute of Science and Innovation in Mechanical and Industrial Engineering
R. Dr. Roberto Frias 400, 4200-465 Porto, Portugal
ana.i.pais@gmail.com, falves@fe.up.pt
[2]ISEP Department of Mechanical Engineering, School of Engineering, Polytechnic of Porto
R. Dr. António Bernardino de Almeida 431, 4200-072 Porto, Portugal
job@isep.ipp.pt

Abstract. The design of bone scaffold involves the consideration of stress shielding which occurs when the Young's modulus of the implant is higher than the Young's modulus of the bone it is replacing and therefore, bone decay occurs in the surrounding tissue. It is therefore very important that the material is adequately adapted to the properties of the surrounding tissue to allow for appropriate load transfer between the bone and the implant. There are several studies to evaluate the occurrence of proper bone ingrowth in scaffold using bone remodelling models and most studies assume an already existing scaffold design.

This work aims at combining meshless methods combined with the bone remodelling algorithm as a way to develop optimized functional gradients of infill density for bone scaffold with the intent of obtaining mechanical properties in the scaffold that will be compatible with bone tissue.

Keywords: finite element method, radial point interpolation method, natural neighbour radial point interpolation method, bio-inspired remodelling algorithm, gyroid

1   Introduction

Bio-scaffold for tissue engineering is a growing application for cellular materials such as the gyroid foam. The gyroid is a triply periodic minimal surface (TPMS) and its adaptation into a foam material presents adequate mechanical properties to fix large bone defects [1, 2]. Thus, combined with adequate density gradients [3] from structural optimization algorithms, it is feasible to match the mechanical properties of bone patch. In this work the gyroid infill properties were obtained experimentally to obtain a law in the form of $E = f(\rho_{app})$, so the homogeneous properties of the material are considered in the optimization.

With regards to the use of bone remodelling and topology algorithms to develop and study bone implants, there are several examples in the literature.

Ghaziani et al. [4] studied a bone growth through a bone remodelling algorithm to test the design of several functionally graded material (FGM) prosthesis. The algorithm uses a strain energy density (SED) based approach, where the density is updated according to the stimulus and Wu et al. [5] evaluated bone ingrowth in the scaffold as a function of the mechanical stimulus. These approaches are concerned with the osteointegration of bone in the implant, by considering previously defined scaffold designs. However, Harrysson et al. [6] in their study mentioned the possibility of using optimization algorithms to develop non-stochastic mesh implants to improve the properties of the hip stem prosthesis.

The approach in this work uses the optimization algorithms, which replicate the bone tissue distribution to adapt the density gradient of the scaffold in a way that will mimic the human bone it is replacing.

2 Materials and methods

2.1 Meshless methods

The two meshless methods applied in this work are the radial point interpolation method (RPIM) and the natural neighbour radial point interpolation method (NNRPIM). While the FEM establishes nodal connectivity through elements, the RPIM and the NNRPIM use different concepts, namely the concept of influence domains.

The RPIM obtains the influence domain by defining a set of nodes in the vicinity of an interest point. The size and shape of the domain will heavily influence the performance of the method. The 3D problems analysed in this work, considered an influence domain containing $n_d = 27$ nodes.

For the NNRPIM, the concept of influence domains is replaced by influence cells which are obtained again from the Voronoi diagram of the nodal distribution. Thus, using the Voronoi it is possible to establish for each node discretizing the problem domain its natural neighbours (i.e., the geometrically closest nodes).

More information on the integration scheme of both methods can be found in [7].

Both the RPIM and the NNRPIM use the Radial Point Interpolators (RPI) technique to construct the interpolating shape functions. The RPI combines a radial basis functions with a polynomial basis functions. Thus, considering an integration point $\boldsymbol{x}_I$ with an influence-domain defined by $X_I = \{\boldsymbol{x}_1, \boldsymbol{x}_2, ... \boldsymbol{x}_n\} \in \mathbb{R}^3$, any variable field $\boldsymbol{u}(\boldsymbol{x}_I)$ can be interpolated at $\boldsymbol{x}_I$ using eq. (1)

$$\boldsymbol{u}(\boldsymbol{x}_I) = \boldsymbol{r}(\boldsymbol{x}_I)^{\mathrm{T}} \boldsymbol{a}(\boldsymbol{x}_I) + \boldsymbol{p}(\boldsymbol{x}_I)^{\mathrm{T}} \boldsymbol{b}(\boldsymbol{x}_I). \tag{1}$$

The multiquadrics radial basis function is used as RBF, thus, $\boldsymbol{r}(\boldsymbol{x}_I)$ can be defined as eq. (2)

$$\boldsymbol{r}_i(\boldsymbol{x}_I) = (d_{iI}^2 + (\gamma \widehat{w}_I)^2)^p, \tag{2}$$

where d_{iI} is the euclidean distance between a node and the interest point and $\widehat{w}_I$ is the integration weight of the point. The MQ-RBF shape parameters γ and p, used in the RPIM were $\gamma = 1.42$ and $p = 1.03$ and in the NNRPIM were $\gamma = 0.0001$ and $p = 0.9999$, which have previously been optimized for best performance [7].

The polynomial based used in the RPIM was linear $\boldsymbol{p}(\boldsymbol{x}) = \{1 \ x \ y \ z\}^{\mathrm{T}}$ and the polynomial base used in the NNRPIM was constant $\boldsymbol{p}(\boldsymbol{x}) = \{1\}^{\mathrm{T}}$

The vectors $\boldsymbol{a}(\boldsymbol{x}_I)$ and $\boldsymbol{b}(\boldsymbol{x}_I)$ represent the non-constant values that must be obtained in order to define the shape function of $\boldsymbol{x}_I$. Applying eq. (1) to each node inside the influence domain and forcing $\boldsymbol{P}\boldsymbol{a}(\boldsymbol{x}_I) = 0$, a set of equations is obtained:

$$\begin{bmatrix} \boldsymbol{R} & \boldsymbol{P} \\ \boldsymbol{P}^{\mathrm{T}} & \boldsymbol{Z} \end{bmatrix} \begin{Bmatrix} \boldsymbol{a}(\boldsymbol{x}_I) \\ \boldsymbol{b}(\boldsymbol{x}_I) \end{Bmatrix} = \boldsymbol{M}_T \begin{Bmatrix} \boldsymbol{a}(\boldsymbol{x}_I) \\ \boldsymbol{b}(\boldsymbol{x}_I) \end{Bmatrix} = \begin{Bmatrix} \boldsymbol{u}_s \\ \boldsymbol{z} \end{Bmatrix}. \tag{3}$$

Thus, the vectors $\boldsymbol{a}(\boldsymbol{x}_I)$ and $\boldsymbol{b}(\boldsymbol{x}_I)$ are obtained and substituting into eq. (1)

$$\boldsymbol{u}_h = \{\boldsymbol{r}(\boldsymbol{x}_I)^{\mathrm{T}} \ \boldsymbol{p}(\boldsymbol{x}_I)^{\mathrm{T}}\} \boldsymbol{M}_T^{-1} \begin{Bmatrix} \boldsymbol{u}_s \\ \boldsymbol{z} \end{Bmatrix} = \{\boldsymbol{\phi}(\boldsymbol{x}_I)^{\mathrm{T}} \ \boldsymbol{\psi}(\boldsymbol{x}_I)^{\mathrm{T}}\} \begin{Bmatrix} \boldsymbol{u}_s \\ \boldsymbol{z} \end{Bmatrix}, \tag{4}$$

it is possible to obtain the RPI shape functions the vector $\boldsymbol{\phi}(\boldsymbol{x}_I)^{\mathrm{T}}$,

$$\boldsymbol{\phi}(\boldsymbol{x}_I) = \Big\{ \phi_1(\boldsymbol{x}_I) \quad \phi_2(\boldsymbol{x}_I) \quad \cdots \quad \phi_n(\boldsymbol{x}_I) \Big\}. \tag{5}$$

2.2 Remodelling algorithm

It is assumed that the trabecular arrangement occurs in the direction of principal stress which corresponds to an optimal configuration for stiffness maximization. This model was adapted by Belinha et al. [7] and combined with meshless methods. The bone remodelling phenomenon is nonlinear. It is presented as a differential equation where a temporal-spatial based functional $\rho_{app}(\boldsymbol{x}, t)$ is minimized with respect to time:

$$\frac{\partial \rho_{app}(\boldsymbol{x}, t)}{\partial t} \cong \frac{\Delta \rho_{app}(\boldsymbol{x}, t)}{\Delta t} = \left(\rho_{app}^{model}\right)_{t_j} - \left(\rho_{app}^{model}\right)_{t_{j+1}} = 0. \tag{6}$$

The temporal domain is discretized in fictitious time steps $t_j \in \mathbb{R}$ where $j \in \mathbb{N}$.

For a fictitious time step t_j, the medium apparent density of the model is given by:

$$\rho_{app}^{model} = Q^{-1} \sum_{i=1}^{Q} (\rho_{app})_I, \tag{7}$$

where $(\rho_{app})_I$ is the apparent density of the interest point $\boldsymbol{x}_I$, defined through $\rho_I = g(\sigma_I)$, being $g(\sigma_I) : \mathbb{R}^3 \mapsto \mathbb{R}$
.

$$g(\sigma_I) = max \left(\{ \sigma_1^{-1}(\rho_I) \ \sigma_2^{-1}(\rho_I) \ \sigma_3^{-1}(\rho_I) \} \right). \tag{8}$$

The stresses σ_1, σ_2 and σ_3 are the principal stresses, and $\sigma_1^{-1}(\rho_I)$, $\sigma_2^{-1}(\rho_I)$ and $\sigma_3^{-1}(\rho_I)$ are the inverse functions of the material law which correlates the apparent stress with the mechanical properties. So, it is possible to obtain equations of the apparent density in an interest point as a function of the stress evaluated in that point.

Said correlations are applied to the points belonging to the following interval:

$$U(\boldsymbol{x}_I) \in [U_m, U_m + \alpha \cdot \Delta U[\cup]U_M - \beta \cdot \Delta U, U_M], \tag{9}$$

which define the set of points being subject to the remodelling process, where U_m is the minimum U and U_M is the maximum U verified. Growth and decay rate of the apparent density are represented by α and β, respectively, and must be defined for each problem, as well as the control density $\rho_{app}^{control}$. When equilibrium is achieved, the remodelling stops.

$$\frac{\Delta \rho}{\Delta t} = 0 \wedge \left(\rho_{app}^{model} \right)_{t_j} = \rho_{app}^{control}. \tag{10}$$

2.3 Homogenized material law

With the experimental results of tensile tests on specimens of the gyroid infill, it was possible to obtain a homogenised Young's modulus for several infill densities of the gyroid infill, which was then associated with the apparent density of the specimen, considering that the density of bulk PLA (E = 3145 MPa) is $\rho_0 = 1.25g/cm^3$. In the end, it was possible to develop a material law for gyroid foam cells correlating the Young's modulus with the apparent density

$$E^{gyr}[MPa] = -482.65\rho_{app}^3 + 938.34\rho_{app}^2 + 27.693\rho_{app}. \tag{11}$$

With the results of experimental compression tests, it was also possible to obtain the ultimate compression stress and correlate such value with the corresponding apparent density

$$\sigma_c^{gyr}[MPa] = -18.853\rho_{app}^3 + 43.021\rho_{app}^2 + 12.242\rho_{app}. \tag{12}$$

In the algorithm, it is with eq. (12) that the inverse functions referred in eq. (8) are obtained, and thus, the apparent density in the points can be actualized. The mechanical properties to obtain the field variables are obtained with eq. (11).

In order to allow a direct comparison of the mechanical behaviour of a structure fabricated with gyroid foam and the same structure made of bone, the following bone tissue phenomenological law was considered [7]:

$$E_{cortical}^{bone}[MPa] = 68357.14\rho_{app}^3 - 276771.43\rho_{app}^2 + 386136.43\rho_{app} - 177644.29, \tag{13}$$

$$E_{trabecular}^{bone}[MPa] = 805.86\rho_{app}^2 + 721.61\rho_{app},\tag{14}$$

$$\sigma_c^{bone}[MPa] = 20.3508\rho_{app}^3 + 26.7984\rho_{app}^2,\tag{15}$$

which was simplified to consider bone tissue as isotropic. As mentioned previously, the density level which marks the threshold between cortical and trabecular bone is $1.3g/cm^3$.

2.4 Remodelling models and boundary conditions

Figure 1 shows the models and the boundary conditions used in the remodelling analysis. The applied loads aim to replicate the most prevalent load case at the proximal femur [7]: the traction load F_1 at the greater trochanter (from the trochanter inserted tendons) and a compression load F_2 at the femur head (from the hip joint). Since at each stage, the design variables are brought to their elastic limit (according to eq. (12)), unitary forces were applied, being that F_1 corresponds to $1/3$ of F_2. For both models, the forces are applied as being vertical (only applied along Oz). The base of the models was pinned. Moreover, it was defined that the base and the area where F_2 is applied are not going to be subject to remodelling, in both models.
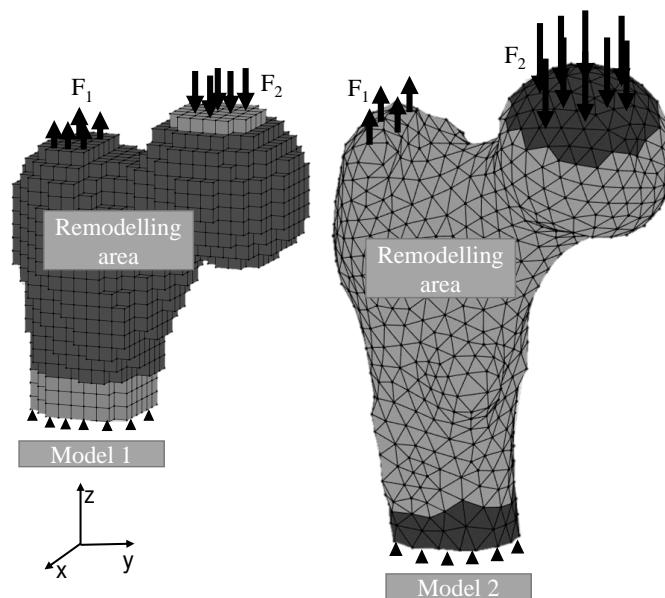
Figure 1. Model 1 (structured), discretized into 3086 nodes and 2284 8-node hexahedral elements; and model 2 (realistic), discretized into 1969 nodes and 9112 4-node tetrahedral elements

The maximum density defined for the gyroid infill corresponds to an infill density of 85% and the minimum density corresponds to an infill density of 10%, because the density of the filament which was used to characterize the gyroid infill is $\rho_0 = 1.25g/cm^3$. The maximum, minimum and transition density values defined for the bone model are correspondent to threshold values for the properties of bone [8].

The remodelling analyses are performed according to a strain energy density criterion, which is a criterion for stiffness maximization. The remodelling parameters used for each of the models are shown in Table 1.

3 Results and discussion

The obtained density fields are shown in Fig. 2 for model 1 and Fig. 3 for model 2, for a mass of 50% of the initial mass. Regarding the structure configuration, both the gyroid material law and the bone tissue material law obtained similar density fields, meaning that the porosity distribution is equivalent. Therefore, it can be evaluated if the functional gradients, naturally occurring in bone tissue, can be mimicked by other materials. This is important

Table 1. Remodelling parameters used in the analysis

Model	Material	β	α	$\rho_{app}[g/cm^3]$		
				maximum	threshold	minimum
1	Gyroid infill	0.05	0.01	1.06	-	0.125
	Bone tissue			2.1	1.3	0.1
2	Gyroid infill	0.025	0.01	1.06	-	0.125
	Bone tissue			2.1	1.3	0.1

since bone tissue scaffold design must also include the study of permeability and porosity (which are important for cell proliferation) and thus, viability of the implant [1, 2, 9].

Moreover, the structure evolved into a configuration that was expected to occur given the load case which leads to bending of the femoral stem.
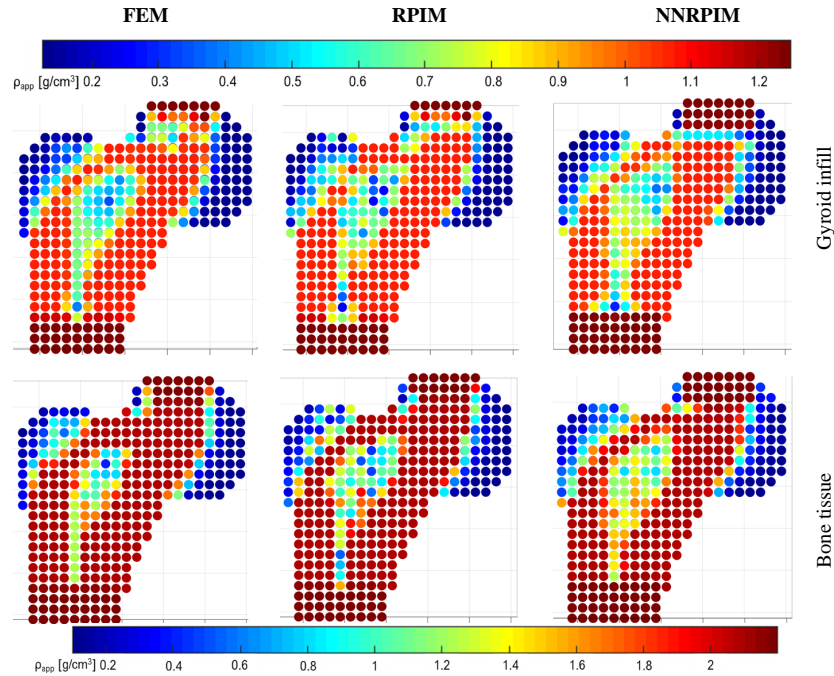
Figure 2. Comparison of gyroid and bone tissue density distribution for a volume fraction of 50% on model 1

The stiffness coefficient K is evaluated as a measure of the scaffold modulus in comparison to the bone it is replacing. With the results of the gyroid scaffold, the values for an implant with the same geometry and built with Ti alloy were approximated through eq. (16), where E_{Ti} is the Young's modulus of titanium (E_{Ti} = 119 GPa), E_{Gyr} is the Young's modulus of the scaffold material, in this case, PLA (E_{Gyr} = 3145MPa) and K_{Gyr} is given by eq. (17)

$$K_{Ti} = \frac{E_{Ti}}{E_{Gyr}} K_{Gyr},$$ (16)

$$K[N/mm] = \frac{\sum_{i=1}^{n_t} (f_z^{top})_i}{\frac{1}{n_t} \sum_{j=1}^{n_t} (d_z^{top})_j},$$ (17)

where in its turn, n_t is the number of nodes, at the top of the femur head where F_2 is applied, f_z is the vertical force applied to each of those nodes and d_z is the vertical displacement of those nodes.

Thus, the plots in Figure 4 were obtained, where it is possible to compare, as a function of apparent density, the difference in modulus of a titanium scaffold and bone tissue.
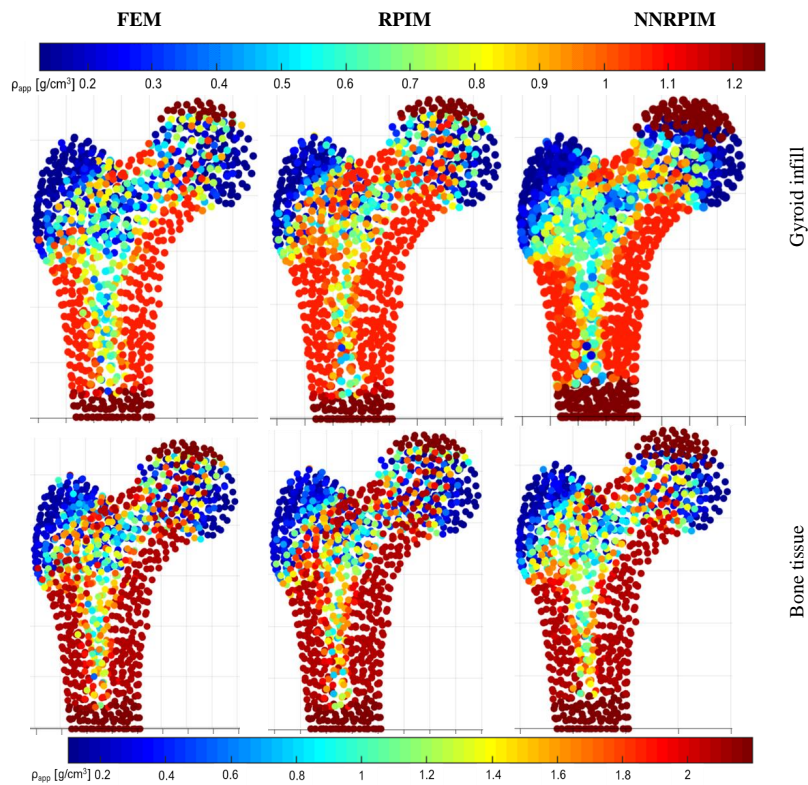
Figure 3. Comparison of gyroid and bone tissue density distribution for a volume fraction of 50% on model 2
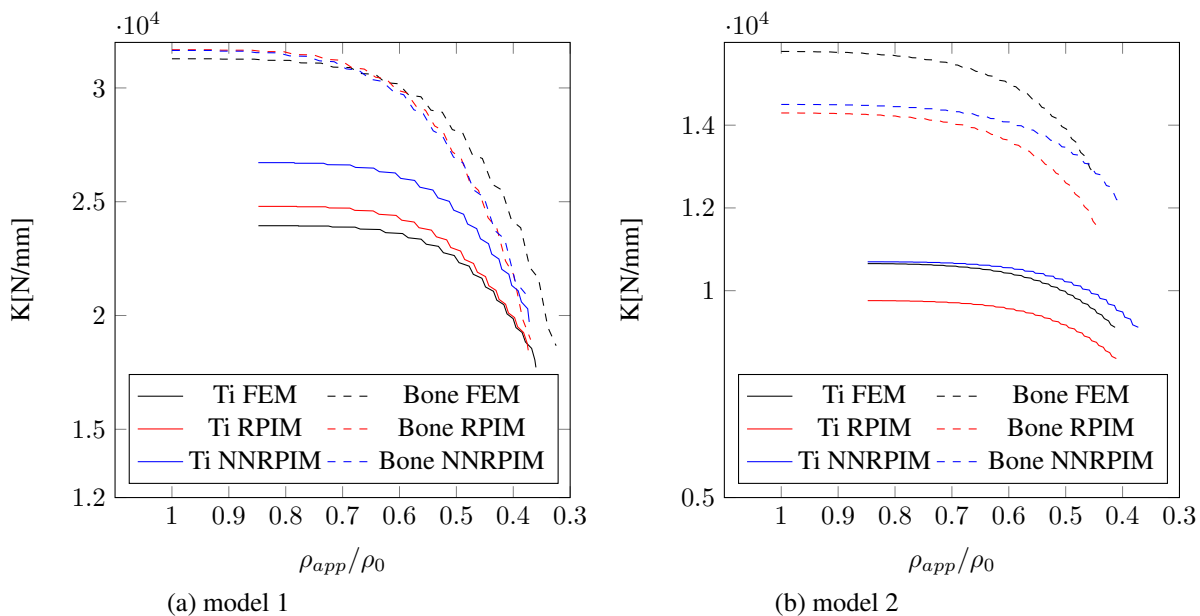
Figure 4. Comparison of the stiffness coefficient of the titanium (Ti) scaffold with bone tissue

Analysing Fig. 4, the stiffness of the titanium scaffold is lower than the stiffness of the bone it is replacing, and thus, it is an adequate material to manufacture the gyroid scaffold. Similar conclusions had been obtained in the study by Bobbert et al. [2]. Due to the properties of the homogenized gyroid model, the stiffness coefficient first decreases slightly and then, decreases more abruptly. Thus, when ρ_{app}^{avg}/ρ_0 reaches 0.6, it is observed a high rate of stiffness loss in the material as the apparent density decreases.

A relevant aspect of the study cannot be obtained by scaling the PLA gyroid scaffold into a Titanium gyroid

scaffold which is the load bearing capability of the implant. Even though the stiffness is lower than bone which allows for proper bone growth, it is necessary that the loads in the human body can be supported by the scaffold. Previous studies in the literature indicate that generally, the apparent strength of scaffolds is sufficient to fill the requirements [1, 2].

4   Conclusions

As its main contribution, this study proposes a framework to obtain functionally graded gyroid foams that can be used to manufacture bone replacement. Here, it is presented a phenomenological material law for PLA gyroid foams that can be scaled to other materials showing a similar linear elastic behaviour. The proposed material law homogenizes the PLA gyroid foam mechanical behaviour, allowing to obtain (as a function of the apparent density of the PLA gyroid foam) the homogenized Young's modulus and ultimate compression stress. It was found that both remodelling algorithms (bio-inspired and bone tissue) achieve similar density patterns, indicating that the bio-inspired remodelling algorithm is suited to approximate functionally graded foam distributions resembling physiological solutions. Meshless methods achieved solutions that are similar to the FEM with the remodelling algorithm.

Authorship statement. The authors hereby confirm that they are the sole liable persons responsible for the authorship of this work, and that all material that has been herein included as part of the present paper is either the property (and authorship) of the authors, or has the permission of the owners to be included here.

References

[1] S. Ma, Q. Tang, Q. Feng, J. Song, X. Han, and F. Guo. Mechanical behaviours and mass transport properties of bone-mimicking scaffolds consisted of gyroid structures manufactured using selective laser melting. *Journal of the Mechanical Behavior of Biomedical Materials*, vol. 93, n. January, pp. 158–169, 2019.

[2] F. S. Bobbert, K. Lietaert, A. A. Eftekhari, B. Pouran, S. M. Ahmadi, H. Weinans, and A. A. Zadpoor. Additively manufactured metallic porous biomaterials based on minimal surfaces: A unique combination of topological, mechanical, and mass transport properties. *Acta Biomaterialia*, vol. 53, pp. 572–584, 2017.

[3] D. Li, W. Liao, N. Dai, G. Dong, Y. Tang, and Y. M. Xie. Optimal design and modeling of gyroid-based functionally graded cellular structures for additive manufacturing. *CAD Computer Aided Design*, vol. 104, pp. 87–99, 2018.

[4] A. O. Ghaziani, R. Soheilifard, and S. Kowsar. The effect of functionally graded materials on bone remodeling around osseointegrated trans-femoral prostheses. *Journal of the Mechanical Behavior of Biomedical Materials*, vol. 118, n. February, pp. 104426, 2021.

[5] C. Wu, J. Fang, A. Entezari, G. Sun, M. V. Swain, Y. Xu, G. P. Steven, and Q. Li. A time-dependent mechanobiology-based topology optimization to enhance bone growth in tissue scaffolds. *Journal of Biomechanics*, vol. 117, n. January, pp. 110233, 2021.

[6] O. L. Harrysson, O. Cansizoglu, D. J. Marcellin-Little, D. R. Cormier, and H. A. West. Direct metal fabrication of titanium implants with tailored materials and mechanical properties using electron beam melting technology. *Materials Science and Engineering C*, vol. 28, n. 3, pp. 366–373, 2008.

[7] J. Belinha. *Meshless Methods in Biomechanics - Bone Tissue Remodelling Analysis*. Springer, Porto, Portugal, 2014.

[8] P. Zioupos, R. B. Cook, and J. Hutchinson. Some basic relationships between density values in cancellous and cortical bone. *Journal of biomechanics*, vol. 41, pp. 1961–1968, 2008.

[9] F. R. Rose and R. O. Oreffo. Bone tissue engineering: Hope vs hype. *Biochemical and Biophysical Research Communications*, vol. 292, n. 1, pp. 1–7, 2002.